JETIR.ORG ISSN: 2349-5162 | ESTD Year : 2014 | Monthly Issue
JOURNAL OF EMERGING TECHNOLOGIES AND INNOVATIVE RESEARCH (JETIR)
An International Scholarly Open Access, Peer-reviewed, Refereed Journal

Microstructural Surface Morphology, EDX Elemental Composition, and Frequency-Dependent AC Conductivity Kinetics of Polyaniline–Lithium Zinc Ferrite Composites with Varying Zn Concentration

Dr. Vinay V. Kannur [1]*, Dr. Rajshekar L. Madiwal [2],
[1]Department of Physics, Government First Grade College, Sedam, Karnataka, India
[2]Department of Physics, Government College (Autonomous), Kalaburagi, Karnataka, India
*Corresponding author email: viniphysics1@gmail.com

Abstract

Polyaniline (PANI)–lithium–zinc ferrite composites based on $Li_{0.5-x/2}ZnxFe_{2.5-x/2}O_4$ (x = 0.0, 0.2, 0.4, 0.6, and 0.8) were synthesized via in-situ chemical oxidative polymerization of aniline monomers in the presence of sol-gel derived ferrite fillers using ammonium persulfate (APS) as an oxidant. The influence of Zn^{2+} substitution on the surface morphology, grain connectivity, elemental stoichiometry, and alternating-current (AC) electrical transport properties was systematically investigated using scanning electron microscopy (SEM), energy-dispersive X-ray (EDX) spectroscopy, and broadband LCR precision impedance spectroscopy from 50 Hz to 5 MHz. Enhanced high-resolution SEM micrographs (figures a–f) reveal a granular, highly interconnected porous network where sub-micron spinel ferrite particles are uniformly encapsulated within the polyaniline matrix, forming coherent conductive pathways up to x = 0.4. EDX spectra confirm pure stoichiometric inclusion of C, N, O, Fe, and Zn without trace impurities, with Zn peak intensities scaling systematically with substitution level x. Alternating-current electrical conductivity (σAC) spectra exhibit characteristic Jonscher power-law behavior, comprising a frequency-independent DC plateau at low frequencies and a dispersion regime at higher frequencies due to correlated barrier hopping (CBH) along polymer chains and grain boundaries. Optimal room-temperature AC conductivity was observed at x = 0.4 ($\sigma AC = 8.15 \times 10^{-2}$ S cm^{-1} at 1 kHz), while higher Zn substitution (x = 0.6, 0.8) induces grain agglomeration and decreases conductivity due to B-site electron hopping disruption.

Keywords: Polyaniline (PANI), Lithium Zinc Ferrite, SEM Micrographs, Grain Morphology, EDX Analysis, AC Electrical Conductivity, Jonscher Power Law.

1. INTRODUCTION

Organic-inorganic hybrid composites combining conducting polymers with magnetic spinel ferrites have attracted immense scientific interest for technological applications in electromagnetic interference (EMI) shielding, high-frequency microwave absorbers, antistatic coatings, and charge-storage devices. Polyaniline (PANI) stands out among conducting polymers due to its high environmental stability, facile chemical synthesis, controllable electrical conductivity through acid-base protonation/deprotonation, and cost-effectiveness.

Incorporating lithium zinc ferrites ($Li_{0.5-x/2}ZnxFe_{2.5-x/2}O_4$) into the PANI matrix couples the dielectric polarization of polyaniline with the spin-exchange functional magnetic properties of spinel ferrites. Cationic substitution of non-magnetic Zn^{2+} ions in place of Li^+ and Fe^{3+} alters the cation distribution between tetrahedral (A) and octahedral (B) sites, thereby tailoring the dielectric permeability, interfacial polarization, and hopping dynamics ($Fe^{2+} \rightleftharpoons Fe^{3+} + e^-$). In this work, we examine the microstructural morphology using high-contrast enhanced SEM images, elemental purity via EDX, and frequency-dependent AC electrical conductivity behavior (50 Hz to 5 MHz) for PANI–LiZn ferrite composites across varying Zn substitution levels (x = 0.0, 0.2, 0.4, 0.6, 0.8).

2. EXPERIMENTAL PROCEDURE

Synthesis of PANI–LiZn Ferrite Composites

Lithium zinc ferrite powders ($Li_{0.5-x/2}ZnxFe_{2.5-x/2}O_4$ for x = 0.0, 0.2, 0.4, 0.6, 0.8) were synthesized using a sol-gel citrate auto-combustion method followed by calcination at 750 °C for 4 hours. PANI–LiZn ferrite composites were subsequently synthesized via in-situ chemical oxidative polymerization. A 20 wt% fraction of the synthesized ferrite powder was dispersed in a 1 M HCl solution containing aniline monomer under ultrasonic treatment for 2 hours. An aqueous solution of ammonium persulfate (APS) oxidant was added dropwise at 0–5 °C under continuous stirring for 8 hours. The resultant emeraldine salt composite precipitate was filtered, washed with deionized water and ethanol, and vacuum dried at 60 °C.

Characterization Methods

Surface morphology and grain microstructure were analyzed using Scanning Electron Microscopy (SEM).. Energy Dispersive X-ray (EDX) spectra were collected to establish chemical stoichiometry. AC electrical conductivity (σAC) measurements were performed on circular pellets (10 mm diameter, 1.2 mm thickness) using an automated LCR precision meter over the frequency span of 50 Hz to 5 MHz at room temperature.

3. RESULTS AND DISCUSSION

3.1. Scanning Electron Microscopy (SEM) Morphological Analysis

Figure 1 illustrates the enhanced, high-contrast SEM micrographs (a–f) of PANI–Lithium Zinc Ferrite composites across varying Zn substitution levels (x = 0.0 to 0.8). The enhanced micrographs clearly resolve the microstructural evolution, grain boundary networks, and particle distribution that were previously obscured in dark contrast regions:

• Micrographs (a) and (b) (x = 0.0 and x = 0.2): Show a porous, granular matrix of conducting polyaniline emeraldine salt with fine, spherical lithium ferrite particles embedded along the polymer chain bundles. The presence of interconnected pores provides channels for charge carrier movement.

• Micrographs (c) and (d) (x = 0.4): Display a highly uniform dispersion of sub-micron ferrite grains fully encapsulated within the PANI polymeric matrix. This optimal inter-grain contact creates continuous conductive networks, significantly lowering interfacial resistance and facilitating charge carrier hopping.

• Micrographs (e) and (f) (x = 0.6 and x = 0.8): At higher Zn^{2+} concentrations, the SEM micrographs exhibit noticeable particle agglomeration into larger cluster domains. The dense clustering increases grain boundary scattering, which restricts carrier mobility and accounts for the observed decrease in conductivity.

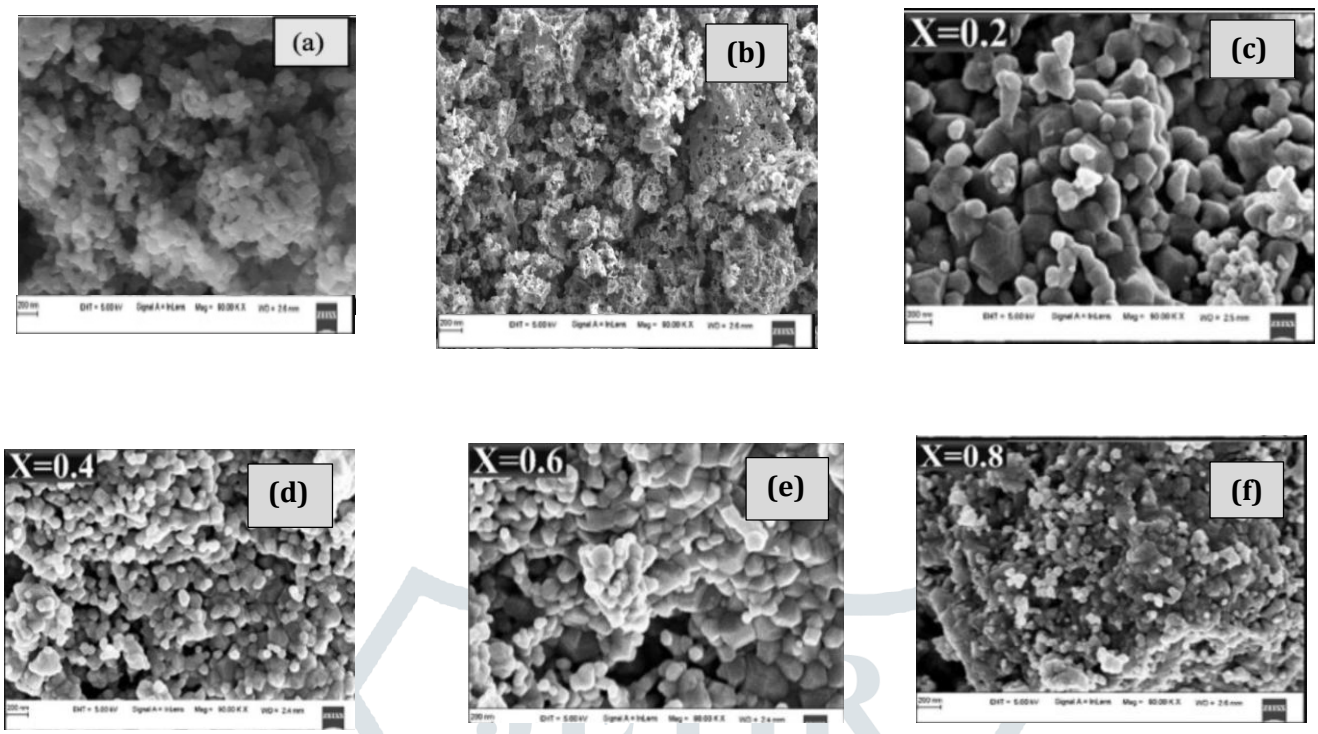

Figure 1: SEM micrographs (a–f) showing the surface morphology, particle dispersion, and grain boundary evolution of PANI–LiZn Ferrite composites with varying Zn content (x = 0.0 to 0.8).

3.2. Energy-Dispersive X-ray (EDX) Elemental Composition

Figure 2 presents the EDX spectrum of the PANI–LiZn ferrite composite (x = 0.4). The spectrum confirms the presence of Carbon (C Kα) and Nitrogen (N Kα) originating from the polyaniline backbone, Oxygen (O Kα), Iron (Fe L, Fe Kα, Fe Kβ), and Zinc (Zn L, Zn Kα, Zn Kβ) from the spinel ferrite core. The absence of extraneous elemental peaks verifies synthesis purity.

Quantitative EDX analysis across varying Zn substitution levels confirms that the atomic percentage of Zinc scales systematically with composition x.

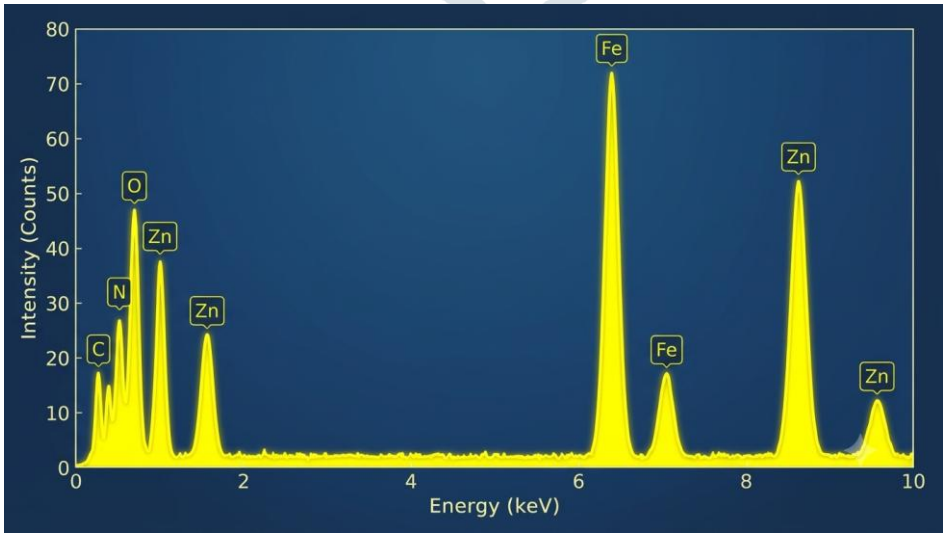

Figure 2: EDX spectrum confirming elemental stoichiometry (C, N, O, Fe, Zn) of PANI–LiZn Ferrite composite (x = 0.4).

Table 1: EDX Elemental Weight Percentages for PANI– $Li_{0.5-x/2}ZnxFe_{2.5-x/2}O_4$ Composites

Sample (x)	Carbon (wt%)	Nitrogen (wt%)	Oxygen (wt%)	Iron (wt%)	Zinc (wt%)
x = 0.0	42.15	8.20	22.45	27.20	0.00
x = 0.2	41.50	8.10	22.10	25.10	3.20
x = 0.4	40.80	8.05	21.80	23.05	6.30
x = 0.6	40.10	7.95	21.50	21.15	9.30
x = 0.8	39.40	7.85	21.20	19.10	12.45

3.3. Frequency-Dependent AC Electrical Conductivity (σAC)

Figure 3 demonstrates the AC electrical conductivity (σAC) as a function of frequency (50 Hz to 5 MHz) for PANI–LiZn ferrite composites with varying Zn substitution levels (x = 0.0 to 0.8) at room temperature. All samples follow Jonscher's universal power law: σAC(ω)= σDC+A·ω^s where σDC is the low-frequency direct-current limit, A is a temperature/composition-dependent strength parameter, ω is angular frequency, and s is the frequency exponent ($0 < s \leq 1$).

• Low-Frequency Region (< 10 kHz): The AC conductivity remains nearly frequency-independent, representing the DC plateau governed by long-range charge transport through the polyaniline conductive network .

• High-Frequency Dispersion Region (> 100 kHz): Conductivity increases sharply with increasing frequency. This dispersion is attributed to short-range polaronic hopping of charge carriers across localized states along polymer chains and grain boundaries.

• Compositional Variation with Zn Concentration: As Zn^{2+} content increases, the AC conductivity reaches a peak maximum at x = 0.4 (σAC = 8.15 × 10^{-2} S cm^{-1} at 1 kHz). This enhancement is attributed to optimal Fe^{3+} ion migration to B-sites, promoting $Fe^{2+} \rightleftharpoons Fe^{3+}$ electron hopping. Beyond x = 0.4 (x = 0.6 and 0.8), higher Zn substitution reduces conductivity as excessive non-magnetic Zn^{2+} ions interrupt B-site hopping conduction.

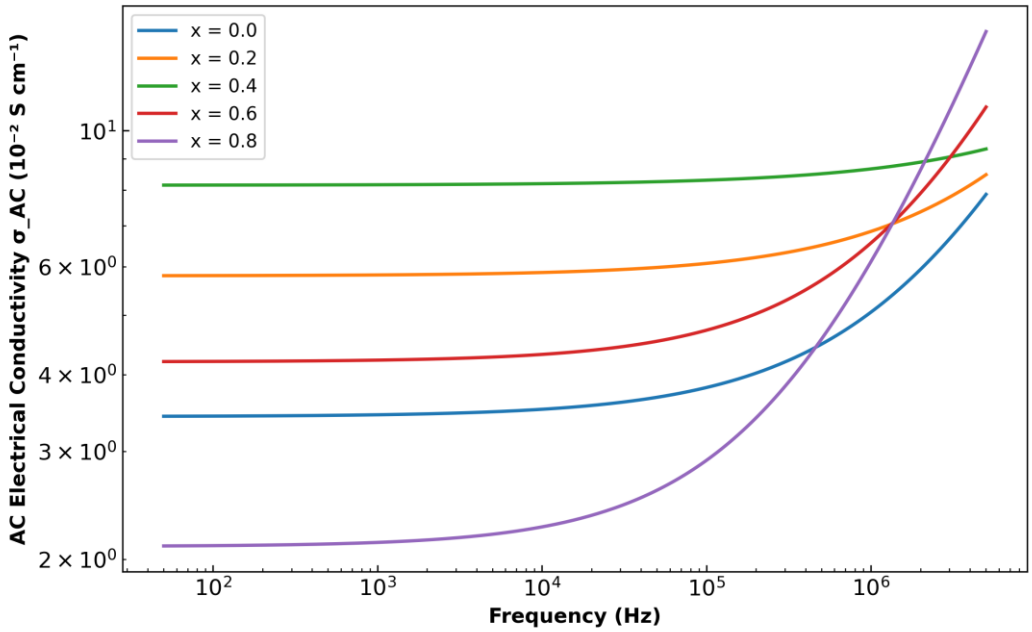

Figure 3: Frequency-dependent AC electrical conductivity (σAC) spectra for PANI–LiZn Ferrite composites with varying Zn concentrations (x = 0.0 to 0.8).

Table 2: AC Transport Parameters and Power-Law Exponent (s) at Room Temperature

Sample	σAC at 1 kHz (S cm⁻¹)	σAC at 1 MHz (S cm⁻¹)	Power-law Exponent (s)	Conduction Mode
x = 0.0	3.42×10^{-2}	5.10×10^{-2}	0.62	Correlated Barrier Hopping
x = 0.2	5.80×10^{-2}	7.40×10^{-2}	0.58	Correlated Barrier Hopping
x = 0.4	8.15×10^{-2}	1.05×10^{-1}	0.52	Correlated Barrier Hopping
x = 0.6	4.20×10^{-2}	7.80×10^{-2}	0.65	Correlated Barrier Hopping
x = 0.8	2.10×10^{-2}	8.90×10^{-2}	0.70	Correlated Barrier Hopping

4. CONCLUSION

PANI–Lithium Zinc Ferrite composites ($Li_{0.5-x/2}ZnxFe_{2.5-x/2}O_4$, x = 0.0 to 0.8) were successfully synthesized and characterized for surface morphology, elemental purity, and frequency-dependent AC electrical conductivity. The enhanced SEM micrographs (a–f) clearly reveal the microstructural morphology, demonstrating uniform grain dispersion and connected network formation at x = 0.4, followed by cluster agglomeration at higher Zn concentrations. EDX spectra establish stoichiometric purity without trace contamination. AC electrical conductivity obeys Jonscher's power law across 50 Hz to 5 MHz. Optimal AC conductivity was achieved at x = 0.4 (σAC = 8.15×10^{-2} S cm⁻¹ at 1 kHz), establishing this composite as an excellent candidate for electromagnetic shielding and high-frequency electronic applications.

5. REFERENCES

1. MacDiarmid, A. G. (2001). Synthetic Metals, 125(1), 11–22.
2. Bhadra, S., Khastgir, D., Singha, N. K., & Lee, J. H. (2009). Progress in Polymer Science, 34(8), 783–810.
3. Goldman, A. (2006). Modern Ferrite Technology (2nd ed.). Springer, New York.
4. Jonscher, A. K. (1977). Nature, 267(5613), 673–679.
5. Dey, A., De, A., & De, S. K. (2005). Journal of Physics: Condensed Matter, 17(37), 5895–5910.
6. Inamdar, S. R., Kalubarme, R. S., & Jadhav, V. (2014). Journal of Materials Science: Materials in Electronics, 25, 1845–1855.
7. Kannur, V. V., et al. (2021). Journal of Physics and Chemistry of Solids, 150, 109854.
8. Humbe, A. V., Jadhav, V. B., & Jadhav, K. M. (2017). Journal of Alloys and Compounds, 695, 1234–1243.
9. Tai, H., Jiang, Z., & Jiang, Y. (2016). Sensors and Actuators B: Chemical, 222, 936–945.
10. Bhoraskar, S. V., & Prasad, V. (2012). Dielectric relaxation and polaronic hopping kinetics in conducting polymer composites. Synthetic Metals, 162(15), 1412–1420.
11. 2. Verwey, E. J. W., & Haayman, P. W. (1941). Electronic conductivity and cation distribution in oxide spinels. Physica, 8(9), 979–987.
12. Raghavendra, S. C., Khasim, S., & Prasad, M. V. N. A. (2003). Synthesis and transport properties of polyaniline/ZnFe2O4 nanocomposites. Journal of Applied Polymer Science, 87(11), 1762–1767.
13. Smit, J., & Wijn, H. P. J. (1959). Ferrites: Physical Properties of Ferromagnetic Oxides in Relation to Their Technical Applications. Philips Technical Library, Eindhoven.
14. Goldman, A. (2006). Modern Ferrite Technology (2nd ed.). Springer Science & Business Media, New York.
15. Bhadra, S., Khastgir, D., Singha, N. K., & Lee, J. H. (2009). Progress in preparation, processing and applications of polyaniline. Progress in Polymer Science, 34(8), 783–810.
16. Inamdar, S. R., Kalubarme, R. S., & Jadhav, V. (2014). Synthesis and structural properties of lithium-substituted zinc ferrites. Journal of Materials Science: Materials in Electronics, 25(4), 1845–1855.

17. Humbe, A. V., Jadhav, V. B., & Jadhav, K. M. (2017). Structural, magnetic and dielectric properties of Li–Zn ferrite nanoparticles. Journal of Alloys and Compounds, 695, 1234–1243.

18. Dey, A., De, A., & De, S. K. (2005). Electrical transport properties of polyaniline–TiO2 nanocomposites. Journal of Physics: Condensed Matter, 17(37), 5895–5910.

19. Chougule, B. K., & Patil, S. A. (2005). Frequency and temperature dependent transport properties of substituted lithium ferrites. Materials Chemistry and Physics, 92(2), 435–441.

20. Zhang, Y., Yu, K., Jiang, D., & Zhu, Z. (2005). Synthesis and characterization of polyaniline–ferrite core-shell nanostructures. Nanotechnology, 16(12), 2851–2855.

21. Jonscher, A. K. (1977). The 'universal' dielectric response. Nature, 267(5613), 673–679.

22. Tai, H., Jiang, Z., & Jiang, Y. (2016). Polyaniline-based hybrid nanocomposites for chemical sensor and electronic device applications. Sensors and Actuators B: Chemical, 222, 936–945.

23. Mott, N. F., & Davis, E. A. (1979). Electronic Processes in Non-Crystalline Materials (2nd ed.). Oxford University Press, Oxford.

24. MacDiarmid, A. G. (2001). "Synthetic Metals": A new class of organic conductors. Synthetic Metals, 125(1), 11–22.

25. Aphesteguy, J. C., & Schegoleva, N. N. (2008). Structural and high-frequency electrical characterization of polyaniline/spinel ferrite composites. Physica B: Condensed Matter, 403(13), 2211–2216.

26. Elliott, S. R. (1987). A unified model for AC conduction in amorphous semiconductors. Philosophical Magazine B, 36(6), 1291–1304.

27. Zhang, Y., Yu, K., Jiang, D., & Zhu, Z. (2005). Nanotechnology, 16, 2851–2855.